Applied Physics Letters ARTICLE pubs.aip.org/aip/apl

Weak ferromagnetism and magnetoelectric coupling in van der Waals antiferromagnet $MnPSe_3$

Cite as: Appl. Phys. Lett. **124**, 172903 (2024); doi: 10.1063/5.0206361
Submitted: 1 March 2024 · Accepted: 16 April 2024 ·
Published Online: 25 April 2024

View Online Export Citation CrossMark

J. H. Zhang,[1,a)] L. Lin,[1,2,a)] S. H. Zheng,[3,a)] P. Z. Chen,[1] L. Huang,[1] G. Z. Zhou,[1] W. J. Zhai,[1] F. Yu,[1] B. Yu,[1] X. M. Cui,[1] M. F. Liu,[3] Y. S. Tang,[4] Z. B. Yan,[1] and J.-M. Liu[1]

AFFILIATIONS

[1]Laboratory of Solid State Microstructures, Nanjing University, Nanjing 210093, China
[2]Department of Applied Physics, College of Science, Nanjing Forestry University, Nanjing 210037, China
[3]Institute for Advanced Materials, Hubei Normal University, Huangshi 435002, China
[4]School of Science, Nanjing University of Posts and Telecommunications, Nanjing 210023, China

[a)]**Authors to whom correspondence should be addressed:** zhangjunhuwdwl3@126.com; llin@njfu.edu.cn; and shzheng@hbnu.edu.cn

ABSTRACT

With the discovery of two-dimensional (2D) ferroelectricity and ferromagnetism in van der Waals (vdW) materials, there has been significant interest in 2D multiferroics. Herein, we report the occurrence of weak ferromagnetism and magnetoelectricity in vdW antiferromagnet $MnPSe_3$ single crystals. Our results demonstrate that $MnPSe_3$ undergoes an antiferromagnetic transition at the Néel temperature $T_N = 70$ K with weak ferromagnetism along the [1–10] direction. Detailed magnetoelectric (ME) data show that $MnPSe_3$ exhibits a linear ME tensor α_{ij} with nine nonzero components. Additionally, a magnetically induced electric polarization as large as 98.5 $\mu C/m^2$ is observed along the [110] direction, with a ME coefficient of 13.5 ps/m at 10 K for a magnetic field of 9 T applied along the [110] direction. Importantly, we discuss our experiments based on symmetry and microscopic analysis, thereby suggesting that the spin-dependent *p-d* hybridization mechanism plays an important role in the emergence of magnetic-field-induced ferroelectricity. Hence, our findings provide insights for exploring the ME coupling in vdW materials.

Published under an exclusive license by AIP Publishing. https://doi.org/10.1063/5.0206361

25 April 2024 14:36:09

Multiferroics, in which more than one ferroic order coexist, have attracted considerable attention owing to their intriguing physics and promising applications in multifunctional devices.[1–5] In the past two decades, substantial efforts have been devoted to designing and searching for single-phase multiferroics with effective cross coupling between the magnetic and ferroelectric orders, such as $TbMnO_3$,[6–8] $Fe_4Nb_2O_9$,[9–11] and Ni_3TeO_6.[12–14] However, owing to the constraining factors like size limitation, interface effects, and dangling bonds, traditional three-dimensional (3D) multiferroic materials have been found difficult to meet the development demands for the miniaturization of electronic devices. Compared with 3D multiferroics, van der Waals (vdW) materials exhibit different physical properties, such as stable layered structure and no surface dangling bonds, making them promising to avoid these issues.[15] Indeed, significant advancements have been made in the field of emergent 2D materials in recent years, such as ferroelectricity in $CuInP_2S_6$ (Ref. 16) and In_2Se_3[17] and ferromagnetism in $Cr_2Ge_2Te_6$ (Ref. 18) and Fe_3GeTe_2.[19] While there are numerous 2D magnets available, the 2D vdW multiferroics with intrinsic coupling between magnetic and ferroelectric orders are yet rare. This has led to the research of 2D vdW multiferroics as a highly prominent research area in recent years.[20–22]

Recently, manganese phosphorous trichalcogenides, namely, $MnPX_3$ (X = S, Se), have attracted extensive studies due to their rich physical properties.[23–26] Among them, $MnPS_3$ crystallizes in monoclinic space group $C2/m$ and undergoes an antiferromagnetic (AFM) transition at temperature $T \sim 78$ K, forming an Ising-type magnetic structure with an angle of 8° between the Mn^{2+} spins and the normal to the *ab* plane.[26] Such a magnetic structure exhibits $2'/m$ symmetry, allowing a linear non-diagonal ME effect. Using optical second harmonic generation (SHG) rotational anisotropy[25] and polarized neutrons,[26] the linear ME effect of $MnPS_3$ has been investigated, but direct evidence for ME coupling is still limited. In this sense, the success in observing the non-diagonal ME phase in $MnPS_3$ stimulates us to further explore the ME effect in $MnPSe_3$.

In contrast to $MnPS_3$, which has out-of-plane magnetic moments, $MnPSe_3$ features in-plane spins with large XY anisotropy, offering richer magnetic domain structures and ME properties.

Published under an exclusive license by AIP Publishing

$MnPSe_3$ crystallizes in centrosymmetric crystal structure with R-3 space group, which can be visualized as the ABCABC stacking of the $Mn_2P_2Se_6$ layer along the c-axis, as plotted by the VESTA software[27] shown in Fig. 1(a). Within each $Mn_2P_2Se_6$ layer, the magnetic Mn ions are arranged in a honeycomb lattice with the ethane-like $[P_2Se_6]^{4-}$ polyanion cluster located in the voids of the honeycomb. Neutron powder diffraction measurements indicate that $MnPSe_3$ undergoes an AFM transition at the temperature $T \sim 72$ K with the magnetic point group of $-1'$, which allows the ME effect with nine nonzero ME components.[28] As shown in Fig. 1(b), the nearest neighboring magnetic moments of Mn^{2+} ions in each layer are antiferromagnetically arranged, while the moments between the adjacent layers are ferromagnetically coupled. The recent SHG study on $MnPSe_3$ as a function of layer thickness demonstrates that such long-range magnetic ordering can persist down to the monolayer limit.[29] Unfortunately, no research has been reported on the ME response in $MnPSe_3$ to date. In this sense, experimental explorations of the ME effect in bulk $MnPSe_3$ through direct measurements are urgently needed for exploring ME devices based on vdW materials.

Motivated by the aforementioned discussion, in this work, we systematically investigate the magnetism and ME coupling in $MnPSe_3$ single crystals by performing a series of magnetic, specific heat, and ME measurements. Our results reveal that $MnPSe_3$ is a linear ME material that exhibits weak ferromagnetism along the [1–10] direction and strong ME effect along the [110] direction. Detailed ME measurements do show that $MnPSe_3$ exhibits a linear ME tensor with nine nonzero ME components, further confirming the magnetic point group of $-1'$ for $MnPSe_3$. Based on the magnetic symmetry of the antiferromagnetic ordering in a honeycomb network and microscopic analysis, the ME coupling mechanism in $MnPSe_3$ is discussed.

Figure 1(c) displays the room-temperature XRD pattern of $MnPSe_3$ single crystal. Using Bragg's law, the layer distance d calculated from the (00l) diffraction peaks is 6.64 Å, in excellent agreement with the value of 6.65 Å in a previous report.[28] The insets in Fig. 1(c) are the optical photograph of an as-grown $MnPSe_3$ single crystal and the Laue diffraction spots obtained along the [001] orientation. Furthermore, the measured EDX spectroscopy reveals the atomic ratio of Mn:P:Se as 0.965:1.062:2.975, consistent with the stoichiometry of $MnPSe_3$. In Fig. 1(d), we show the Rietveld refined XRD pattern of the crushed crystals, in which all the diffraction peaks can be well fitted by R-3 space group with lattice parameters $a = b = 6.4891$ Å and $c = 20.0479$ Å, consistent with a previous report.[28]

Figure 2(a) presents the T-dependent magnetic susceptibility $\chi(T)$ curves under zero-field-cooling (ZFC) mode with the measuring field $H = 0.1$ T applied along the [110], [1–10], and [001] directions, namely $\chi_{[110]}$ and $\chi_{[1\text{–}10]}$, and $\chi_{[001]}$, respectively. Upon cooling from

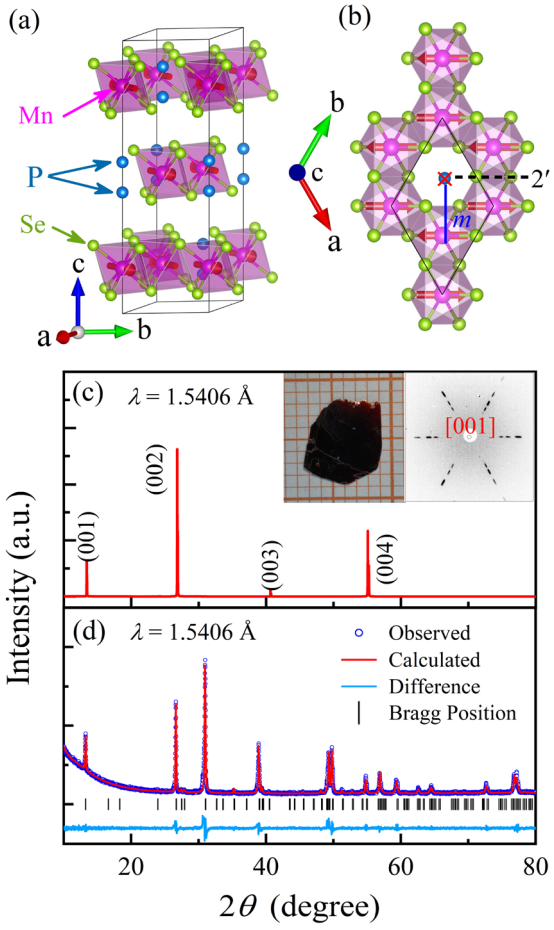


FIG. 1. (a) The crystal and magnetic structure of $MnPSe_3$, drawn based on Ref. 28. The red arrows present the magnetic moment of Mn^{2+} ions. (b) Top view of the magnetic structure of a Mn^{2+} honeycomb layer. The dashed black line denotes the twofold symmetry plus time-reversal symmetry, the solid blue line and the symbol × denotes the mirror and $-1'$ symmetry, respectively. (c) Room-temperature XRD pattern of $MnPSe_3$, the insets are the photograph of as-grown single crystal and Laue diffraction spots obtained along the [001] direction. (d) The Rietveld refinement of room-temperature XRD data of the crushed $MnPSe_3$ crystals.

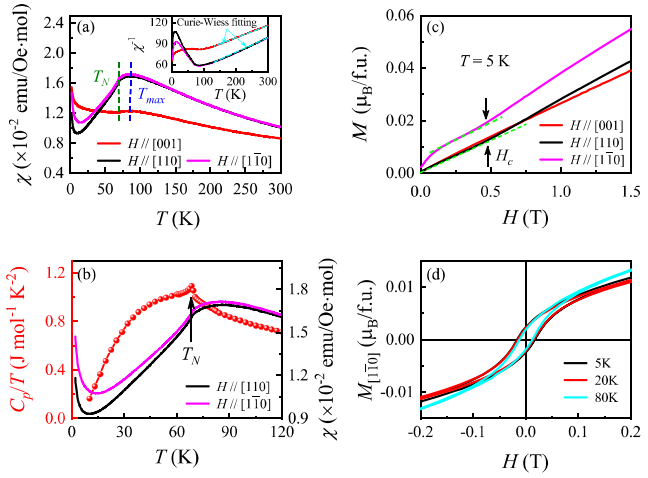


FIG. 2. (a) The T dependence of magnetic susceptibility (χ) along the [110], [1–10], and [001] directions. The inset shows the Curie–Weiss fitting of χ^{-1} between 150 and 300 K. (b) The T dependence of special heat C_p/T, susceptibility $\chi_{[110]}$, and $\chi_{[1\text{–}10]}$ curves. (c) Magnetization along the [110], [1–10], and [001] directions at $T = 5$ K. (d) The H dependence of magnetization along the [1–10] direction measured at several selected temperatures. The dashed blue and olive lines in (a) the temperature point T_N and T_{max}. The dashed green lines in (c) are used to show the linear relationship.

25 April 2024 14:36:09

Published under an exclusive license by AIP Publishing

300 K, the in-plane susceptibilities $\chi_{[110]}$ and $\chi_{[1-10]}$ gradually increase to their maximum at $T = T_{max} = 85$ K and then decrease, followed by a kink observed at $T \sim 70$ K. Given the quasi-two-dimensional nature of $MnPSe_3$, the broad peak suggests the emergence of AFM ordering. With further decrease in temperature, susceptibilities $\chi_{[110]}$ and $\chi_{[1-10]}$ display a gradual drop, with $\chi_{[110]}$ exhibiting a sharper decrease. On the other hand, the $\chi_{[001]} - T$ curve demonstrates a weak T-dependence, implying that the magnetic moments are mainly lying in the ab-plane with the easy-axis along the [110] direction. Furthermore, the significant disparity between the in-plane and out-of-plane $\chi(T)$ curves indicates the pronounced XY anisotropy of $MnPSe_3$.[30]

By fitting the linear part of the $\chi^{-1}(T)$ data between $T = 150$ and 300 K using the Curie–Weiss law, the effective magnetic moments along three directions labeled in the subscript can be obtained, and they are $\mu_{[110]} \sim 6.2$, $\mu_{[1-10]} \sim 6.1$, and $\mu_{[001]} \sim 6.1$ μ_B/Mn, respectively, very close to the spin-only magnetic moment of 5.97 μ_B for Mn^{2+} in the high-spin configuration, where μ_B represents the Bohr magnetic moment. In addition, the corresponding Curie–Weiss temperatures are $\theta_{[110]} \sim -163$, $\theta_{[1-10]} \sim -157$, and $\theta_{[001]} \sim -318$ K, respectively, indicating that the dominant magnetic interactions are antiferromagnetic. The large difference in the Curie–Weiss temperature between the in-plane and out-of-plane direction may be due to the large ligand spin–orbit contribution of the heavier selenium.[30] To further characterize the magnetic transition of $MnPSe_3$, the special heat (C_p/T) under zero field was measured, shown in Fig. 2(b), where the $\chi(T)$ curves with measuring field H applied along the [110] and [1–10] directions are also plotted for reference. The typical λ-shaped peak is observed at $T \sim 70$ K, which denotes the Néel temperature T_N, indicating the onset of long-range AFM ordering. Apart from this ordering, no other $C_p(T)$ anomaly over the whole T range is identified.

To obtain more details of the magnetic properties of $MnPSe_3$, the H-dependent magnetization along the [110], [1–10], and [001] directions are measured at various temperatures. The magnetization M at 5 K shown in Fig. 2(c) exhibits linear behavior below the critical magnetic field $H_c \sim 0.5$ T for H//[110] and [1–10]. Beyond this point, a significant deviation from the linear behavior can be observed. Above $H \sim 1.0$ T, all the $M(H)$ curves show linear behavior. Such a nonlinear deviation of $M(H)$ is also observed in other ME materials such as $Co_4Nb_2O_9$ (Ref. 31) and $Fe_4Nb_2O_9$,[11] which can be attributed to the realignment of three types of magnetic domains and the reorientation of spins within it. Owing to the triple symmetry of $MnPSe_3$ along the c-axis, the [100] direction is equivalent to [010] and [110] directions. Consequently, three types of magnetic domains may also exist, and the nonlinear derivation of $M(H)$ curves can also be attributed to the realignment of magnetic domains with spin reorientation. In contrast to the linear behavior observed in the $M_{[110]}(H)$ curve for $H < H_c$, the $M_{[1-10]}(H)$ curve shows a significant nonlinear behavior below 0.1 T with a magnitude larger than that of $M_{[110]}(H)$ and $M_{[001]}(H)$. Figure 2(d) presents the $M_{[1-10]}(H)$ curves in low field region $H < 0.2$ T at various temperatures. The observable noteworthy hysteresis suggests weak ferromagnetism along the [1–10] direction with a coercive field of $H_{cv} = 167$ Oe. Keeping in mind that the spins are antiferromagnetically aligned along the [110] direction, it can be inferred that the weak ferromagnetism along the [1–10] direction most likely originates from the canted antiferromagnetic order caused by the Dzyaloshinskii–Moriya interaction.

We now turn our attention to the ME effect in the $MnPSe_3$ single crystals. Given the complexity of magnetic domains, the [110] magnetic domain is selected to investigate the ME effect in $MnPSe_3$, in which the magnetic moments are antiferromagnetically aligned along the [110] direction. To analyze the ME tensor, the x, y, and z axes are designed along the [110], [1–10], and [001] directions, respectively. Figures 3(a)–3(c) present the T-dependent pyroelectric current density $J(T)$ along the [001] direction under selected H applied along different orientations. Consistent with long-range antiferromagnetic ordering appearing at $T \sim 70$ K, the sharp peaks in $J_{[001]}(T)$ curves are observed at 71.5 K, indicating the emergence of magnetic-induced ferroelectric polarization. Moreover, by reversing E, a change in the sign of the $J_{[001]}(T)$ curves is observed, shown in the inset of Fig. 3(a), indicating the nature of ferroelectricity of the magnetic-field-induced polarization.

To investigate the ME effect in $MnPSe_3$, we performed comprehensive T-dependent polarization measurements along P// [110], [1–10], and [001] directions under different H orientations, shown in Figs. 3(d)–3(l). Here, several interesting features deserve highlighting. First, our measurements show that the ME tensor of $MnPSe_3$ exhibits nine nonzero components, consistent with the magnetic point group $-1'$ determined by the powder neutron diffraction measurements. Second, under the magnetic field $H = 9$ T applied along the [110] and [1–10] directions, the measured $P_{[110]}$ and $P_{[1-10]}$ at 10 K reach up to 98, 75, and 63, 35 $\mu C/m^2$, respectively, which are larger than the value of 13 and 12 $\mu C/m^2$ for H//[001], indicating the

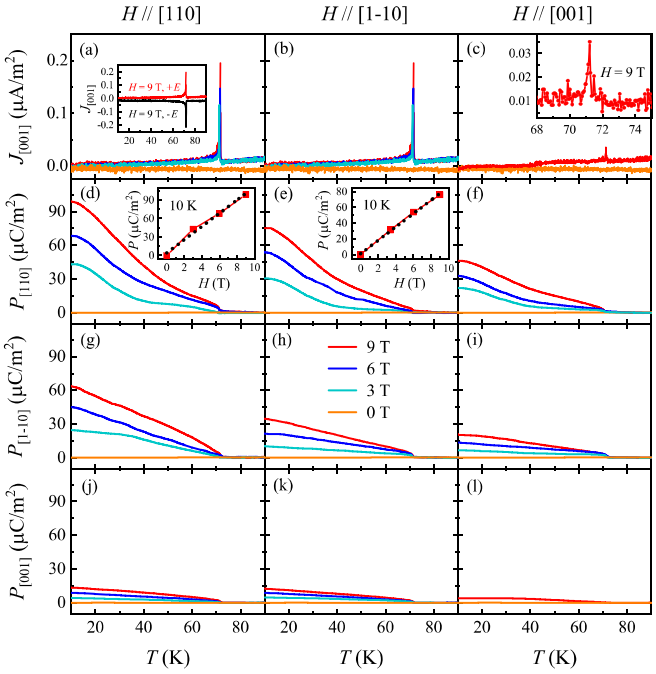


FIG. 3. (a) The T dependence of pyroelectric current density $J_{[001]}$ along the [001] direction in the magnetic field applied along (a) [110], (b) [1–10], and (c) [001] directions, respectively. The inset in (a) shows the T dependence of $J_{[001]}$ collected at $H = 9$ T under different poling electric fields (±20 kV/cm). The inset of (c) displays the $J_{[001]}$ data around 71 K with $H = 9$ T applied along the [001] direction. (d)–(l) The T dependence of electric polarization in the magnetic and poling electric field are applied alternately along [110], [1–10], and [001] directions. The inset in (d) and (e) plots the H-dependent polarization $P_{[110]}$ at 10 K for H//[110] and H//[1–10], respectively.

25 April 2024 14:36:09

Published under an exclusive license by AIP Publishing

majority of polarization is along the [110] direction. Taking the $P_{[110]}$ data at 10 K for H//[110] and H//[1–10] and plotting them as a function of H, one can obtain the ME response $P(H)$ curves, shown in the inset of Figs. 3(d) and 3(e). By fitting the $P(H)$ curves with $P = \alpha H$, the ME coefficients of α_{xx} and α_{xy} are determined to be 13.8 and 10.6 ps/m, respectively, which are comparable to the reported linear ME materials, such as $MnTiO_3$ ($\alpha \sim 2.6$ ps/m),[32] Cr_2O_3 ($\alpha \sim 4.13$ ps/m),[33] and Sm_2BaCuO_5 ($\alpha \sim 4.4$ ps/m).[34] Third, no matter which direction the ferroelectric polarization is along, the polarizations under H//[001] are always smaller than the ones measured under H//[110] and [1–10] directions. This may be attributed to the large XY anisotropy of the magnetic structure that can be more easily changed under the H applied along the *ab* plane.

Finally, we would like to give some qualitative discussion on the ME coupling in $MnPSe_3$. As shown in Fig. 1(a), the crystal structure of $MnPSe_3$ can be seen as the ABCABC stacking of the $Mn_2P_2Se_6$ layer along the *c*-axis. Within each $Mn_2P_2Se_6$ layer, the Mn^{2+} spins are antiferromagnetically aligned along the [110] direction, exhibiting the $2'/m$ and hidden $-1'$ symmetry, shown in Fig. 4(a). Here, $2'$ is the twofold symmetry along the [110] plus a time-reversal symmetry, m is the mirror symmetry perpendicular to [110] direction. Owing to the presence of $-1'$ symmetry, no macroscopic polarization can be expected in the ground state, i.e., $H = 0$. However, when the applied magnetic fields along the [110] and [1–10] directions exceed the critical field H_c, three types of magnetic domains realign into single one with the spins reoriented perpendicularly to H. Consequently, the $-1'$ symmetry breaks and macroscopic ferroelectric polarization emerges. For example, when H//[110] and $H > H_c$, the twofold axis 2//[110] can be unchanged, while the symmetry $m' \perp$ [110] breaks, giving rise to electric polarization along the [110] direction, shown in Fig. 4(b). Similarly, as shown in Figs. 4(c) and 4(d), the application of H//[1–10] and [001] retains $2'$//[110] but breaks $m \perp$ [110], leading to the electric polarization appearing along the [110] direction. To summarize, based on our magnetic symmetric analysis, an application of a magnetic field along three axes always induces the electric polarization along the [110] direction, implying the largest electric polarization can be expected along the [110] direction. Experimentally, the major electric polarization of $MnPSe_3$ is indeed along the [110] direction for H// [110], [1–10], and [001], although a smaller [1–10] component is observed.

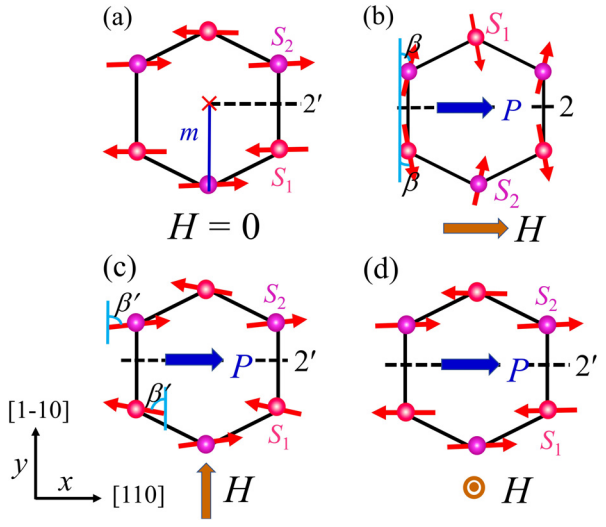


FIG. 4. The magnetic structure and induced electric polarization P under the magnetic field H: (a) $H = 0$, (b) H//[110], (c) H//[1–10], and (d) H//[001]. The dashed blank lines in (a)–(d) represent the $2'$ (or 2) symmetry of spins along the [110] direction, the solid blue line symbol × in (a) represent the mirror and $-1'$ symmetry. The solid light-blue lines in (b) and (c) represent the *x*-axis. The red arrows in (a)–(d) indicate the Mn^{2+} spins, S_1 and S_2 represent the two Mn sites in the honeycomb layer.

Subsequently, we will discuss the possible microscopic origin of ME coupling in $MnPSe_3$. Up to now, the magnetic-induced electric polarization can be explained by three well-known mechanisms: (1) the spin current mechanism,[35] (2) the exchange striction mechanism,[36] and (3) the spin-dependent *p-d* hybridization mechanism.[37] However, in the honeycomb network consisting of six Mn^{2+} spins, the first two mechanisms are not in work since the summary of the vector spin chirality $S_i \times S_j$ in each honeycomb is zero, and the $S_i \cdot S_j$ for all the Mn–Mn bonds are uniform, where S_i and S_j is the magnetic moments at neighboring sites. In the spin-dependent *p-d* hybridization mechanism, a local electric polarization $\Delta p \propto (S \cdot r_l)^2 r_l$ between the transition metal and the ligand can be induced through the spin–orbit coupling, where S is the magnetic moment of the transition metal ion, and r_l is the vector connecting the transition metal and the lth ligand. As the Mn^{2+} ions are located in a noncentrosymmetric environment with threefold symmetry along the *c*-axis, a local electric dipole moment is generated in each $MnSe_6$ octahedron.

As illustrated in Figs. 4(a)–4(d), the magnetic structure of each honeycomb network in $MnPSe_3$ can be represented by two different sites S_1 and S_2, depending on the environment of Mn^{2+} ions and their magnetic moment direction. Each site consists of three Mn^{2+} ions and forms an equilateral triangular. Thus, the local electric polarization $P_{S1}(P_{S2})$ for $S_1(S_2)$ sites can be obtained by the superposition of three local dipoles at $S_1(S_2)$ sites, while the total electric polarization P of each honeycomb network is the superposition of P_{S1} and P_{S2}. According to Ref. 11, the local electric polarization for S_1 and S_2 sites can be expressed as

$$P_{S1} = 3\begin{bmatrix} A\sin^2\alpha_1\cos 2\beta_1 + C\sin 2\alpha_1\cos\beta_1 \\ A\sin^2\alpha_1\sin(-2\beta_1) + C\sin 2\alpha_1\sin\beta_1 \\ C_1\sin^2\alpha_1 + C_2\cos^2\alpha_1 \end{bmatrix},$$
$$P_{S2} = -3\begin{bmatrix} A\sin^2\alpha_2\cos 2\beta_2 + C\sin 2\alpha_2\cos\beta_2 \\ A\sin^2\alpha_2\sin(-2\beta_2) + C\sin 2\alpha_2\sin\beta_2 \\ C_1\sin^2\alpha_1 + C_2\cos^2\alpha_2 \end{bmatrix}, \quad (1)$$

where A, C, C_1, and C_2 are the coupling constants correlated with the structure parameter of MnSe6 octahedral, $\alpha_1(\alpha_2)$ is the angle of the spins at $S_1(S_2)$ site with respect to the *z*-axis, $\beta_1(\beta_2)$ is the angle of the projection of S on the *xy* plane with respect to the *x*-axis.

As shown in Fig. 4(a), in the ground state, the Mn^{2+} ions related by the inversion symmetry have oppositely directed magnetic moments. As a result, the local electric dipoles arising from the spin-dependent *p-d* hybridization mechanism are antiferroelectrically aligned, thereby leading to an absence of macroscopic polarization. For H//[110] and $H > H_c$, the spin directions $\alpha_1, \alpha_2, \beta_1, \beta_2$ can be expressed as $\alpha_1 = -\alpha_2 = 90°$, $\beta_1 = -\beta_2 = \beta$, shown in Fig. 4(b). Putting these relations into Eq. (1), the total polarization can be expressed as

25 April 2024 14:36:09

Published under an exclusive license by AIP Publishing

$$P = P_{S1} + P_{S2} = \begin{bmatrix} P^x \\ P^y \\ P^z \end{bmatrix} = -6A \begin{bmatrix} 0 \\ \sin 2\beta \\ 0 \end{bmatrix}. \quad (2)$$

Similarly, for $H//[1\text{–}10]$ and $H > H_c$, as shown in Fig. 4(c), one can obtain the angle relation as $\alpha_1 = -\alpha_2 = 90°$, $\beta_1 = -\beta_2 = \beta'$. Consequently, the total polarization can be expressed as

$$P = P_{S1} + P_{S2} = \begin{bmatrix} P^x \\ P^y \\ P^z \end{bmatrix} = -6A \begin{bmatrix} 0 \\ \sin 2\beta' \\ 0 \end{bmatrix}. \quad (3)$$

It is important to note from Eqs. (2) and (3) that the electric polarization along the [110] direction is proportional to $\sin 2\beta$ (or $\sin 2\beta'$). For a weak external magnetic field H, the canting angle β (or β') is small, and $\sin 2\beta$ (or $\sin 2\beta'$) $\propto H$ is expected; hence, the linear ME effect appears. However, for $H//[001]$, the spins will tilt to H, i.e., the c-axis, resulting in the angle relations $\alpha_1 = -\alpha_2 = \alpha$, $\beta_1 = -\beta_2 = 90°$, as shown in Fig. 4(d). Substituting these relations into Eq. (1), one can obtain the total polarization $P = 0$, implying no electric polarization can be generated by the spin-dependent p-d hybridization mechanism for $H//[001]$. Our microscopic analysis shows that the major electric polarization along the [110] direction can be obtained through the spin-dependent p-d hybridization mechanism for $H//[110]$ and $[1\text{–}10]$.

In conclusion, we have presented our systematic investigation of the magnetism and ME effect in $MnPSe_3$ single crystals. Our study demonstrates that $MnPSe_3$ is a linear ME material with weak ferromagnetism along the [1–10] direction and strong ME coupling along the [110] direction. The observation of nine nonzero components of the ME tensor aligns with the magnetic point group $-1'$ as determined by powder neutron diffraction measurements. Importantly, our symmetry and microscopic origin analyses suggest that the spin-dependent p-d hybridization mechanism plays an important role in the emergence of magnetically induced ferroelectricity. This work sheds light on the exploration of 2D multiferroic materials as well as the development of next-generation functional nanodevices based on 2D van der Waals materials.

See the supplementary material for the experimental details, the refined parameters obtained from Rietveld refinement, energy-dispersive x-ray spectroscopy mapping images, and the spectrum of $MnPSe_3$ single crystals.

This work was financially supported by the National Key Projects for Basic Researches of China (Grant Nos. 92163210, 12274231, 12304119, 12304124, 12074111, and 52272108).

AUTHOR DECLARATIONS

Conflict of Interest

The authors have no conflicts to disclose.

Author Contributions

J. H. Zhang: Conceptualization (lead); Data curation (lead); Formal analysis (lead); Writing – original draft (equal). **L. Lin:** Conceptualization (equal); Writing – original draft (equal); Writing – review & editing (equal). **S. H. Zheng:** Data curation (equal); Funding acquisition (equal). **P. Z. Chen:** Data curation (equal); Formal analysis (equal). **L. Huang:** Formal analysis (equal). **G. Z. Zhou:** Formal analysis (equal). **W. J. Zhai:** Data curation (equal). **F. Yu:** Formal analysis (equal). **B. Yu:** Formal analysis (equal). **X. M. Cui:** Formal analysis (equal). **M. F. Liu:** Formal analysis (equal). **Y. S. Tang:** Formal analysis (equal). **Z. B. Yan:** Formal analysis (equal); Funding acquisition (equal). **J.-M. Liu:** Formal analysis (equal); Writing – review & editing (equal).

DATA AVAILABILITY

The data that support the findings of this study are available from the corresponding authors upon reasonable request.

REFERENCES

[1] S.-W. Cheong and M. Mostovoy, "Multiferroics: A magnetic twist for ferroelectricity," Nat. Mater. **6**, 13 (2007).
[2] Y. Tokura, S. Seki, and N. Nagaosa, "Multiferroics of spin origin," Rep. Prog. Phys. **77**, 076501 (2014).
[3] S. Dong, J.-M. Liu, S.-W. Cheong, and Z. F. Ren, "Multiferroic materials and magnetoelectric physics: Symmetry, entanglement, excitation, and topology," Adv. Phys. **64**, 519 (2015).
[4] M. Fiebig, T. Lottermoser, D. Meier, and M. Trassin, "The evolution of multiferroics," Nat. Rev. Mater. **1**, 16046 (2016).
[5] C. Lu, M. Wu, L. Lin, and J. M. Liu, "Single-phase multiferroics: New materials, phenomena, and physics," Natl. Sci. Rev. **6**, 653 (2019).
[6] T. Goto, T. Kimura1, H. Shintani, K. Ishizaka, T. Arima, and Y. Tokura, "Magnetic control of ferroelectric polarization," Nature **426**, 55–58 (2003).
[7] I. Aupiais, M. Mochizuki, H. Sakata, R. Grasset, Y. Gallais, A. Sacuto, and M. Cazayous, "Colossal electromagnon excitation in the non-cycloidal phase of $TbMnO_3$ under pressure," npj Quant. Mater. **3**, 60 (2018).
[8] T. Aoyama, K. Yamauchi, A. Iyama, S. Picozzi, K. Shimizu, and T. Kimura, "Giant spin-driven ferroelectric polarization in $TbMnO_3$ under high pressure," Nat. Commun. **5**, 4927 (2014).
[9] A. Maignan and C. Martin, "$Fe_4Nb_2O_9$: A magnetoelectric antiferromagnet," Phys. Rev. B **97**, 161106(R) (2018).
[10] R. Jana, D. Sheptyakov, X. Y. Ma, J. A. Alonso, M. C. Pi, A. Muñoz, Z. Y. Liu, L. L. Zhao, N. Su, S. F. Jin, X. B. Ma, K. Sun, D. F. Chen, S. Dong, Y. S. Chai, S. L. Li, and J. G. Cheng, "Low-temperature crystal and magnetic structures of the magnetoelectric material $Fe_4Nb_2O_9$," Phys. Rev. B **100**, 094109 (2019).
[11] J. H. Zhang, Y. S. Tang, L. Lin, L. Y. Li, G. Z. Zhou, B. Yang, L. Huang, X. Y. Li, G. Y. Li, S. H. Zheng, M. F. Liu, M. Zeng, D. Wu, Z. B. Yan, X. K. Huang, C. Chen, X. P. Jiang, and J.-M. Liu, "Electric polarization reversal and nonlinear magnetoelectric coupling in the honeycomb antiferromagnet $Fe_4Nb_2O_9$," Phys. Rev. B **107**, 024108 (2023).
[12] Y. S. Oh, S. Artyukhin, J. J. Yang, V. Zapf, J. W. Kim, D. Vanderbilt, and S.-W. Cheong, "Non-hysteretic colossal magnetoelectricity in a collinear antiferromagnet," Nat. Commun. **5**, 3201 (2014).
[13] J. W. Kim, S. Artyukhin, E. D. Mun, M. Jaime, N. Harrison, A. Hansen, J. J. Yang, Y. S. Oh, D. Vanderbilt, V. S. Zapf, and S. W. Cheong, "Successive magnetic-field-induced transitions and colossal magnetoelectric effect in Ni_3TeO_6," Phys. Rev. Lett. **115**, 137201 (2015).
[14] J. H. Zhang, L. Lin, Y. S. Tang, G. Z. Zhou, L. Huang, X. Y. Li, G. Y. Li, S. H. Zheng, M. F. Liu, X. M. Liu, Z. B. Yan, X. K. Huang, C. Chen, X. P. Jiang, and J. M. Liu, "Large tunability of the magnetoelectric effect in the Co-substituted polar antiferromagnet Ni_3TeO_6," Phys. Rev. B **108**, 024107 (2023).
[15] X. Tang and L. Z. Kou, "Two-dimensional ferroic and multiferroics: Platforms for new physics and applications," J. Phys. Chem. Lett. **10**, 6634 (2019).
[16] F. Liu, L. You, K. L. Seyler, X. Li, P. Yu, J. Lin, X. Wang, J. Zhou, H. Wang, and H. He, "Room-temperature ferroelectricity in $CuInP_2S_6$ ultrathin flakes," Nat. Commun. **7**, 12357 (2016).
[17] Y. Zhou, D. Wu, Y. H. Zhu, Y. J. Cho, Q. He, X. Yang, K. Herrera, Z. D. Chu, Y. Han, M. C. Downer, H. L. Peng, and K. J. Lai, "Out-of-plane piezoelectricity and ferroelectricity in layered α-In_2Se_3 nanoflakes," Nano Lett. **17**, 5508 (2017).

25 April 2024 14:36:09

Published under an exclusive license by AIP Publishing

[18]C. Gong, L. Li, Z. Li, H. Ji, A. Stern, Y. Xia, T. Cao, W. Bao, C. Wang, Y. Wang, Z. Q. Qiu, R. J. Cava, S. G. Louie, J. Xia, and X. Zhang, "Discovery of intrinsic ferromagnetism in two-dimensional van der Waals crystals," Nature **546**, 265 (2017).
[19]Y. Deng, Y. Yu, Y. Song, J. Zhang, N. Z. Wang, Z. Sun, Y. Yi, Y. Z. Wu, S. Wu, J. Zhu, J. Wang, X. H. Chen, and Y. Zhang, "Gate-tunable room-temperature ferromagnetism in two-dimensional Fe_3GeTe_2," Nature **563**, 94 (2018).
[20]H. Ju, Y. Lee, K. T. Kim, I. H. Choi, C. J. Roh, S. Son, P. Park, J. H. Kim, T. S. Jung, J. H. Kim, K. H. Kim, J. G. Park, and J. S. Lee, "Possible persistence of multiferroic order down to bilayer limit of van der Waals material NiI_2," Nano Lett. **21**, 5126 (2021).
[21]Q. Song, C. A. Occhialini, E. Ergecen, B. Ilyas, D. Amoroso, P. Barone, J. Kapeghian, K. Watanabe, T. Taniguchi, A. S. Botana, S. Picozzi, N. Gedik, and R. Comin, "Evidence for a single-layer van der Waals multiferroic," Nature **602**, 601 (2022).
[22]X. Wang, Z. Shang, C. Zhang, J. Kang, T. Liu, X. Wang, S. Chen, H. Liu, W. Tang, Y. J. Zeng, J. Guo, Z. Cheng, L. Liu, D. Pan, S. Tong, B. Wu, Y. Xie, G. Wang, J. Deng, T. Zhai, H. X. Deng, J. Hong, and J. Zhao, "Electrical and magnetic anisotropies in van der Waals multiferroic $CuCrP_2S_6$," Nat. Commun. **14**, 840 (2023).
[23]X. Zhang, X. Zhao, D. Wu, Y. Jing, and Z. Zhou, "$MnPSe_3$ monolayer: A promising 2D visible-light photohydrolytic catalyst with high carrier mobility," Adv. Sci. **3**, 1600062 (2016).
[24]R. Basnet, K. M. Kotur, M. Rybak, C. Stephenson, S. Bishop, C. Autieri, M. Birowska, and J. Hu, "Controlling magnetic exchange and anisotropy by nonmagnetic ligand substitution in layered MPX_3 (M = Ni, Mn; X = S, Se)," Phys. Rev. Res. **4**, 023256 (2022).
[25]H. Chu, C. J. Roh, J. O. Island, C. Li, S. Lee, J. Chen, J. G. Park, A. F. Young, J. S. Lee, and D. Hsieh, "Linear magnetoelectric phase in ultrathin $MnPS_3$ probed by optical second harmonic generation," Phys. Rev. Lett. **124**, 027601 (2020).
[26]E. Ressouche, M. Loire, V. Simonet, R. Ballou, A. Stunault, and A. Wildes, "Magnetoelectric $MnPS_3$ as a candidate for ferrotoroidicity," Phys. Rev. B **82**, 100408(R) (2010).
[27]K. Momma and F. Izumi, "VESTA 3 for three-dimensional visualization of crystal, volumetric and morphology data," J. Appl. Crystallogr. **44**, 1272 (2011).
[28]S. Calder, A. V. Haglund, A. I. Kolesnikov, and D. Mandrus, "Magnetic exchange interactions in the van der Waals layered antiferromagnet $MnPSe_3$," Phys. Rev. B **103**, 024414 (2021).
[29]Z. Ni, A. V. Haglund, H. Wang, B. Xu, C. Bernhard, D. G. Mandrus, X. Qian, E. J. Mele, C. L. Kane, and L. Wu, "Imaging the Neel vector switching in the monolayer antiferromagnet $MnPSe_3$ with strain-controlled Ising order," Nat. Nanotechnol. **16**, 782 (2021).
[30]P. Jeevanandam and S. Vasudevan, "Magnetism in $MnPSe_3$: A layered $3d^5$ antiferromagnet with unusually large XY anisotropy," J. Phys.: Condens. Matter **11**, 3563 (1999).
[31]L. Ding, M. Lee, T. Hong, Z. L. Dun, R. Sinclair, S. X. Chi, H. K. Agrawal, E. S. Choi, B. C. Chakoumakos, H. D. Zhou, and H. B. Cao, "Noncollinear magnetic structure and magnetoelectric coupling in buckled honeycomb $Co_4Nb_2O_9$: A single-crystal neutron diffraction study," Phys. Rev. B **102**, 174443 (2020).
[32]N. Mufti, G. R. Blake, M. Mostovoy, S. Riyadi, A. A. Nugroho, and T. T. M. Palstra, "Magnetoelectric coupling in $MnTiO_3$," Phys. Rev. B **83**, 104416 (2011).
[33]H. Wiegelmann, A. G. M. Jansen, P. Wyder, J.-P. Rivera, and H. Schmid, "Magnetoelectric effect of Cr_2O_3 in strong static magnetic fields," Ferroelectrics **162**, 141 (1994).
[34]G. Z. Zhou, J. W. Gong, X. Li, M. F. Liu, L. Y. Li, Y. Wang, J. H. Min, J. Liu, D. Cai, F. Liu, S. H. Zheng, Y. S. Tang, Z. C. Xu, Y. L. Xie, L. Yang, M. Zeng, Z. B. Yan, B. W. Li, X. Z. Wang, and J.-M. Liu, "Large magnetoelectric effect in the polar magnet Sm_2BaCuO_5," Appl. Phys. Lett. **115**, 252902 (2019).
[35]H. Katsura, N. Nagaosa, and A. V. Balatsky, "Spin current and magnetoelectric effect in noncollinear magnets," Phys. Rev. Lett. **95**, 057205 (2005).
[36]I. A. Sergienko, C. Şen, and E. Dagotto, "Ferroelectricity in the magnetic E-phase of orthorhombic perovskites," Phys. Rev. Lett. **97**, 227204 (2006).
[37]T.-H. Arima, "Ferroelectricity induced by proper-screw type magnetic order," J. Phys. Soc. Jpn. **76**, 073702 (2007).

25 April 2024 14:36:09

Published under an exclusive license by AIP Publishing